*Desalination and Water Treatment*
www.deswater.com

doi: 10.5004/dwt.2017.21361

89 (2017) 197–209
September

# Preparation and characterization of magnetic $CaFe_2O_4$ nanoparticles for efficient adsorption of toxic Congo Red dye from aqueous solution: predictive modeling by artificial neural network

Akash Deb[a], M. Kanmani[a], Animesh Debnath[a], Kartick Lal Bhowmik[b], Biswajit Saha[b,*]

[a]*Department of Civil Engineering, National Institute of Technology Agartala, Jirania, West Tripura 799046, India, Tel. +918837309890; email: akashdeb341@gmail.com (A. Deb), Tel. +919677240499; email: kanmani.ar@gmail.com (M. Kanmani), Tel. +8575015404; email: debnathanimesh@gmail.com (A. Debnath)*

[b]*Department of Physics, National Institute of Technology Agartala, Jirania, West Tripura 799046, India, Tel. +919436569904; email: biswajit.physics@gmail.com (B. Saha), Tel. +9863585412; email: karticklalb@gmail.com (K.L. Bhowmik)*

Received 27 April 2017; Accepted 25 August 2017

**ABSTRACT**

In this study, the performance and effectiveness of magnetic $CaFe_2O_4$ nanoparticles prepared by simple chemical route were evaluated for the adsorption of toxic azo dye Congo Red (CR) from aqua matrix. The prepared $CaFe_2O_4$ nanoparticles were characterized by X-ray diffraction, scanning electron microscopy, transmission electron microscopy, Fourier transform infrared spectroscopy, vibrating sample magnetometer, point of zero charge, and Brunauer–Emmett–Teller surface area measurements. Batch mode adsorption experiments were performed to study the effect of various experimental parameters namely solution pH (4.0–10.0), contact time (2–120 min), adsorbent dose (0.25–1.5 g/L), and initial CR dye concentration (20–150 mg/L) on the adsorption process. Maximum CR dye removal of 99.01% was achieved at solution pH 4.0 and maximum adsorption capacity of 241.16 mg/g was reported at optimum experimental condition. The adsorption equilibrium data strictly follows Langmuir isotherm model and adsorption kinetics was well described by pseudo-second-order model. A three layered artificial neural network (ANN) was applied for the accurate prediction of percentage of CR dye removal by the $CaFe_2O_4$ nanoparticles. The Levenberg–Marquardt backpropagation algorithm with "tansig" and "purelin" transfer function in hidden and output layer was used for model development. Optimal ANN architecture (4–9–1) shows high $R^2$ value ($R^2$: 0.995) and very low mean squared error value (0.00042866), confirming the accurate prediction ability of CR dye removal efficiency in this adsorption process.

*Keywords:* Congo Red; $CaFe_2O_4$ nanoparticles; Adsorption; Isotherm and kinetic studies; Artificial neural network modeling

## 1. Introduction

Nowadays, aquatic ecosystems are disturbed to a level of no rejuvenation due to indiscriminate disposal of toxic chemical compounds to the aquatic environment through industrial effluents. Many industrial effluents contain toxic organic dyes which are a major water pollutant and have created concern among government and environmentalists since past few decades. Dye loaded wastewater is mainly generated from industries such as textile, leather, paper, printing, and plastic [1,2]. Dyes have become the center of discussion as a water pollutant due to its peculiar properties like (i) resistance to fading on exposure to light, (ii) an aesthetic pollutant whose presence interfere with light penetration in waterbody [3], (iii) inert to biological degradation [4,5], (iv) significantly affect the physicochemical properties of freshwater, and (v) hazardous in nature which exhibit toxic effect to microbial's and carcinogenic to human being [6]. Therefore, these toxic dyes must be removed before

* Corresponding author.

getting discharged into water systems, to decrease their toxic effects on all forms of life. Among azo group of dyes, Congo Red (CR) dye is a well-known carcinogen which forms benzidine after metabolization [7], is considered as a model dye in this research. CR possess a great threat due to its high water solubility and self-assembling capacity in water which produces supramolecular entities stabilized by π–π interactions between aromatic rings and its complex structure makes it highly resistant toward biological degradation [8]. Many different treatment methods have been developed to remove dyes which are arguemented to be adapted under various conditions like strength of pollutant, economics, technical assistance, flexibility, etc. Some of them are electrocoagulation [9], photocatalytic oxidation [10], ion-exchange, chemical oxidation, nanofiltration, and adsorption [11,12]. Among these methods, adsorption has been widely used for dye removal from wastewater for its simplicity, high efficiency, adsorbent versatility, low operating cost, and less sludge production [13]. A wide variety of adsorbents like activated carbon [14], extracellular polymeric substances [15], zero-valent iron nanocomposite [16], biosorbents [17], other natural adsorbents, and waste materials from agricultural waste industries [18,19] have been studied in the recent past for efficient removal of dye from contaminated water. However, these adsorbents possess few drawbacks like low adsorption capacity, high cost for their preparation, difficulties in disposal, and regeneration. With the advent of nanotechnology, nanoscale adsorbents have gained momentum these days which have overcome the above disadvantages and proving to be quite promising for removal of wide variety of water pollutants. Particularly, nanoscale adsorbents with magnetic properties have made a difference from other metallic nanoadsorbents due to their size in nanorange, superparamagnetism, easy synthesis, coating or modification, low toxicity, chemical inertness, biocompatibility [20,21], and most evidently easy separation under external magnetic fields [22]. Some of the magnetic nanoparticles (MNPs) which have already been reported as potential adsorbents are mesostructured silica magnetite, magnetic iron–nickel oxide, montmorillonite-supported MNPs, polyethylenimine-coated $Fe_3O_4$ MNPs, δ-FeOOH-coated γ-$Fe_2O_3$ MNPs, flower-like iron oxides, hydrous iron oxide MNPs, amino-modified $Fe_3O_4$ MNPs, magnetic $Ni_{0.5}Zn_{0.5}Fe_2O_4$ nanopowders, $MgFe_2O_4$ nanoparticles, etc. [21,22]. Out of several magnetic metal ferrites, $CaFe_2O_4$ nanoparticles have wide applications over other MNPs due to its biocompatibility, low toxicity, adjustable magnetic property [23,24], and it also has considerable application in other areas such as cancer therapy, magnetic refrigeration systems, heat transfer applications, drug targeting, magnetic cell separation, enzyme immobilization catalysis, etc. [24].

As discussed earlier, in this research $CaFe_2O_4$ nanoparticles were synthesized via a simple chemical route and its potentiality was studied as adsorbent for remediation of CR dye from aqua matrix. Batch mode adsorption experiments were conducted to analyze the impact of several experimental parameters like solution pH, contact time, initial CR dye concentration, and $CaFe_2O_4$ dose onto the CR dye uptake efficiency. Various kinetic models like pseudo-first-order, pseudo-second-order, and intra-particle diffusion model were studied to find the underlying mechanism for adsorption of CR on $CaFe_2O_4$ nanoparticles and isotherm models like Langmuir and Freundlich were also studied to understand the nature of equilibrium of the reactions. Furthermore, popular mathematical tool artificial neural network (ANN)-based predictive modeling was also performed so as to predict the CR dye removal efficiency accurately using batch mode adsorption data as inputs to the model. The above mentioned studies reveal that the $CaFe_2O_4$ nanoparticles can appear as a profound adsorbent for CR dye exploring the novelty of the work based on simplicity of its synthesis, larger effective surface area due to smallness in grain size, and crystalline nature. Furthermore, this work has the merits of additive free, and low-cost synthesis process of $CaFe_2O_4$ nanoparticles for faster adsorption of CR dye, confirming the applicability of synthesized adsorbent for environmental application.

## 2. Materials and methods

### 2.1. Chemicals and reagents

High purity chemicals were used in this research work without any refinement. CR dye, ferric chloride anhydrous ($FeCl_3$), hydrochloric acid (HCl), sodium hydroxide (NaOH) pellets, and calcium chloride dihydrate ($CaCl_2.2H_2O$) were purchased from Merck (India), and all solutions were prepared using deionized (DI) water (Millipore, 18 MΩ·cm) in total experimental procedure.

### 2.2. Synthesis and characterization of adsorbent

A typical chemical precipitation process was employed for the growth of $CaFe_2O_4$ nanoparticles using $CaCl_2.2H_2O$ and $FeCl_3$ as the calcium and iron source, respectively, and sodium hydroxide as precipitating agent. The stepwise flowchart for $CaFe_2O_4$ nanoparticles synthesis is depicted in Fig. 1. To obtain $CaFe_2O_4$, 12.0 g of $FeCl_3$ and same amount of $CaCl_2.2H_2O$ were blended in 250 mL DI water in two separate beakers till the clear suspensions were obtained. These two solutions were then added to another beaker containing a homogenous solution of NaOH prepared by blending 20.0 g of NaOH pellets in 500 mL DI water. This mixing results to heavy brownish suspension which was separated by filtration and then dried. The dried materials were washed several times with DI water for removal of impurities and thereafter annealed at 200°C for 8 h to get the desired nanoparticles.

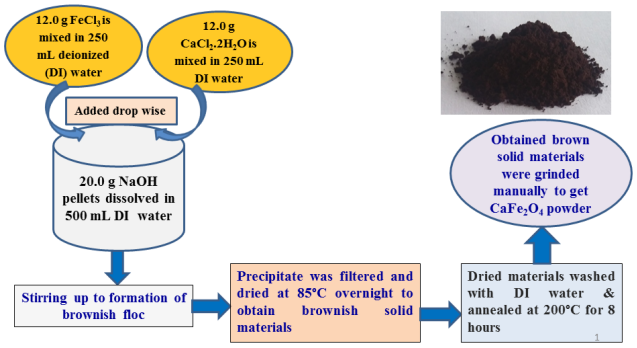


Fig. 1. Flowchart showing the simple chemical route synthesis process of $CaFe_2O_4$ nanoparticles.

The prepared $CaFe_2O_4$ nanoparticles were characterized by X-ray diffraction (XRD), scanning electron microscopy (SEM), transmission electron microscopy (TEM), vibrating sample magnetometer (VSM), point of zero charge (PZC), Fourier transform infrared spectroscopy (FTIR), and Brunauer–Emmett–Teller (BET) surface area measurements. An SEM (FE-SEM, Hitachi, S-4800) and X-ray diffractometer (Bruker, D-8 Advance) were used to characterize the surface and anatomical property. The morphology of prepared $CaFe_2O_4$ nanoparticles was studied using TEM, JEOL TEM-3010, while FTIR measurement was carried out by FTIR (PerkinElmer-Spectrum 400). BET surface area of the prepared adsorbent was measured by a Quanta Chrome Nova-1000 instrument and PZC was measured using typical pH drift method using 0.01 M KCl solution as background electrolyte. At room temperature, VSM measurements were performed by a Lakeshore, Model: 7410 series instrument.

### 2.3. Methodology for CR dye adsorption

Initially, stock solution of CR dye (500 mg/L) was prepared and diluted to desired concentrations by successive dilutions with DI water. Concentration of CR dye in the solution after adsorption reaction was determined spectrophotometrically by UV/Vis spectrophotometer (Hach DR 5000) at its maximum absorbency at 498 nm. pH of the working solution was adjusted to desired values using 0.1 M NaOH/HCl. The effect of experimental parameters was studied by varying one parameter at a time and keeping other constant. All the experimental parameters were varied in wide range namely adsorbent dose (0.25–1.5 g/L), initial CR concentration (20–150 mg/L), and initial pH (4.0–10.0) at different time intervals (2, 5, 10, 15, 20, 30, 40, 60, 80, 100, and 120 min). After the completion of adsorption experiment for a predefined time, the adsorbent was separated by using an external magnet and supernatant was used for further analysis.

## 3. Results and discussions

### 3.1. Characterizations of $CaFe_2O_4$ nanoparticles

Fig. 2(a) indicates the XRD pattern of prepared $CaFe_2O_4$ nanoparticles. The diffraction pattern demonstrates several important peaks at 2θ = 29.29°, 31.65°, 32.91°, 45.38°, and 56.44°, which corresponds to reflection from (310), (230), (320), (231), and (431) miller planes of $CaFe_2O_4$ nanoparticles. The Scherrer formula was used to find the crystallite size of the prepared $CaFe_2O_4$ nanoparticles and was found to be 37 nm. Fig. 2(b) indicates the SEM image of $CaFe_2O_4$ nanoparticles. From the SEM image, it is clearly evident that the prepared samples contain non-uniform distribution of particles with various sizes ranging from 50 to 200 nm or so. In addition to smallness in size, presence of voids could also be observed in the samples, which confirms the possibilities of having high surface area and pore volume as good and strong recommended requirement for efficient adsorbent. Fig. 3(a) displays the TEM image of $CaFe_2O_4$ nanoparticles, which displays that the particles are in quasi-spherical shape with grain size of 100–200 nm range. The FTIR spectrum of $CaFe_2O_4$ nanoparticles is shown in Fig. 3(b), which shows several important peaks. The broad range peak at ~3,454 $cm^{-1}$ is due to O–H stretching vibrations and the peak at 1,634 $cm^{-1}$ is due to O–H bending vibrations. The peaks at 875 and 712 $cm^{-1}$ are accredited to Fe–OH and O–Fe–O, however, the peak looked at 1,421 $cm^{-1}$ may be due to C-H bending vibration. The peaks occurring at lower wavelength region (525 and 494 $cm^{-1}$) can be ascribed to the metal oxygen vibrational modes due to Ca–O stretching vibrations of $CaFe_2O_4$, and peaks at 624 and 566 $cm^{-1}$ are ascribed to Fe–O bonds because of the occurrence of ferrite skeleton. BET surface area and pore volume of prepared $CaFe_2O_4$ nanoparticles were analyzed by $N_2$ adsorption–desorption isotherm as shown in Fig. 3(c). The prepared adsorbent has shown high specific surface area of 230 $m^2/g$ and as well as high pore volume of 0.144 $cm^3/g$ with average pore diameter of 2.53 nm, which confirm the potentiality of prepared nanoparticles as an

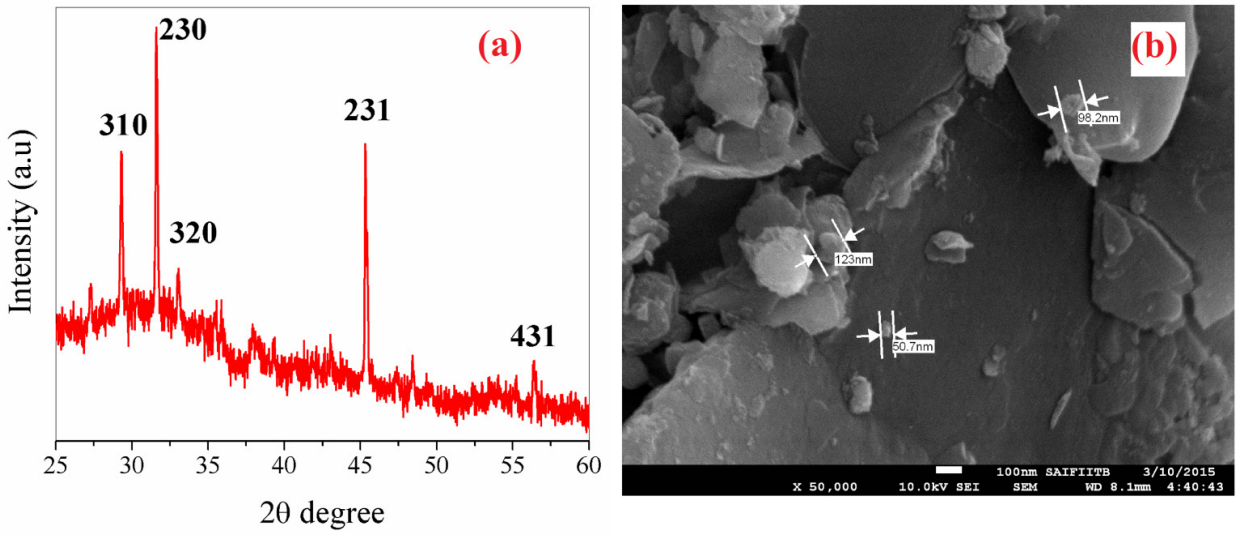


Fig. 2. (a) XRD pattern and (b) SEM image of $CaFe_2O_4$ nanoparticles.

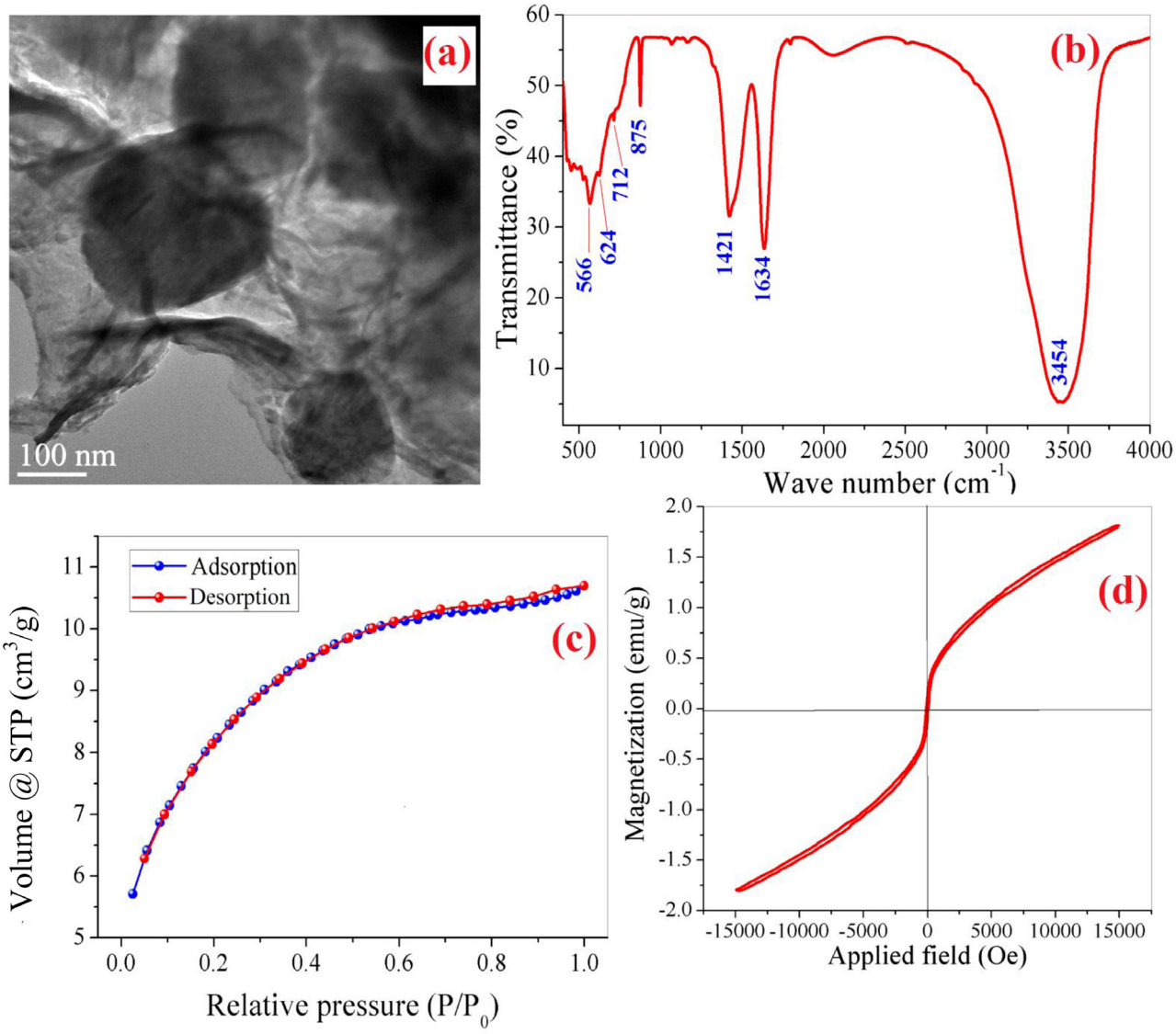


Fig. 3. (a) TEM image; (b) FTIR spectrum; (c) $N_2$ adsorption–desorption isotherm and (d) VSM plot of $CaFe_2O_4$ nanoparticles.

efficient adsorbent for removal of organic dyes. VSM measurement (Fig. 3(d)) revealed that the prepared nanoparticle is magnetically soft in nature and the presence of hysteresis is small at room temperature. As prepared $CaFe_2O_4$ nanoparticles have shown saturation magnetization and coercivity of 1.83 emu/g and 77.22 Oe, respectively, which makes it a potential MNP for efficient separation from water within 30 s under external magnetic field.

### 3.2. Influence of solution pH on CR dye adsorption

The influence of the initial solution pH of the CR solution on its adsorption efficiency by $CaFe_2O_4$ nanoparticles is shown in Fig. 4(a). It can be clearly seen that the adsorption process is highly pH dependent and maximum adsorption efficiency observed at solution pH 4.0. The adsorption efficiency decreased continuously with increase of solution pH in the range of pH 4.0–10.0. CR is an anionic dye which contains negative sulfonic groups ( $SO_3^-$ ) [25]. At solution pH 4.0, strong electrostatic attraction between anionic form of CR dye and positively charged surface of $CaFe_2O_4$ nanoparticles is the main driving force. The positive surface charge of adsorbent at solution pH 5.0 or below can be explained with the view point of PZC of $CaFe_2O_4$ nanoparticles, which is shown in Fig. 4(b). PZC plot indicates that at solution pH below 5.15, the adsorbent surface will be positively charged (PZC = 5.15). The lower pH leads to an increase in $H^+$ ion concentration and the adsorbent surface becomes more positively charged. On the other hand CR undergoes tautomerization due to acidic condition led to the formation of zwitterionic form of CR (protons are attached to the azonium group and the ammonium nitrogen of CR molecule) which is cationic in nature hence a very low adsorption was reported in the solution pH 2.0–4.0 [26]. As the solution pH increases, the number of positively charged sites decreases and negatively charged sites increases. These negatively charged sites do not favor

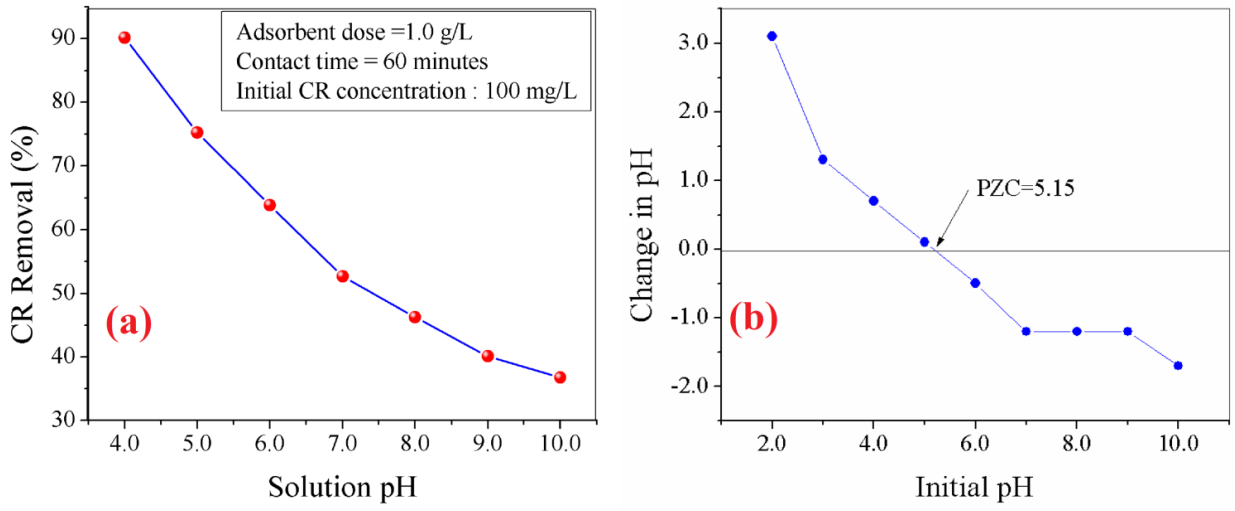


Fig. 4. (a) Effect of solution pH on the adsorption of CR dye, (b) point of zero charge measurement of $CaFe_2O_4$ nanoparticles.

the adsorption of anionic dye due to the electrostatic repulsion [27]. Hence, solution pH was optimized very carefully. The adsorption mechanism is therefore mainly based on the electrostatic attraction between protonated surfaces of adsorbent and anionic part of CR dye. The probable schematic diagram for the interaction mechanism between protonated $CaFe_2O_4$ nanoparticles surface and anionic CR dye molecule is shown in Fig. 5, where strong hydrogen bonding is shown due to conversion of $-SO_3^-$ to $-SO_3H$ at lower solution pH. In view of above, solution pH was kept fixed at 4.0 throughout this study for analysis of other experimental parameters and also for equilibrium and kinetic studies [28,29].

### 3.3. Effect of initial CR dye concentration and contact time

The effect of initial CR dye concentration on the percentage removal and adsorption capacity of the adsorbent is shown in Fig. 6(a). It can be seen that the initial concentration of CR was varied from 20 to 150 mg/L, which led to the decrease in percentage removal of CR from 98.98% to 70.23%. This may be due to the reduction in the available adsorption site of the adsorbent due to the increase in concentration of adsorbate in the aqueous media. However, increase in adsorption capacity was observed from 19.79 to 105.34 mg/g with the increase of initial CR concentration from 20 to 150 mg/L. It is very evident that the initial concentration of dye has a positive effect of overcoming the resistance between the dye from bulk liquid phase to the adsorbent solid phase and hence leading to the higher mass transfer to the surface of the solid phase later to its pores [30], which is validated too in this study.

Fig. 6(b) shows the effect of contact time on the removal efficiency of the CR at fixed adsorbent dose, optimized pH of 4.0, for different initial CR concentrations (20–150 mg/L). It can be observed that after 40 min the reaction was very near to equilibrium with maximum removal efficiency of ~90% and ~55% for initial concentration of 20 and 150 mg/L of CR, respectively, and at 60 min all CR dye solutions were reached to equilibrium. Different concentration of CR shows different percentage removal due to the effect of initial concentration and available active sites to be occupied by CR, but after 60 min due to the repulsive nature between adsorbed CR and CR left in aqueous media the reaction tend to reach equilibrium.

### 3.4. Effect of adsorbent dose

The effect of $CaFe_2O_4$ nanoparticles dose on the adsorption of CR dyes in aqueous solution was studied by varying the $CaFe_2O_4$ nanoparticle dose from 0.25 to 1.5 g/L at fixed solution pH and initial concentration of CR (Fig. 7). Fig. 7 depicts that the removal efficiency of CR dye increases in a steady rate from 60.29% to 99.01% with the increase of the adsorbent dose from 0.25 to 1.5 g/L. This can be attributed to the fact that increase in $CaFe_2O_4$ nanoparticle dose increases the number of binding sites lead to the increase of CR removal efficiency [31,32] with constant initial concentration of CR. But adsorption capacity decreases steeply with increase in adsorbent dose might be due to the overlapping of active surface sites. The overlapping of active surface sites may result to increase in diffusion path length which reduces the adsorption capacity of $CaFe_2O_4$ nanoparticles at higher dose [23].

### 3.5. Kinetic modeling

The kinetic studies were performed to understand the mechanism by which the adsorption occurs and also to know about the rate-limiting step. Moreover, kinetic studies will provide important information for the design of dynamic adsorption system for field application. Pseudo-first-order, pseudo-second-order, and intra-particle diffusion models were used to analyze the batch experiment data for this kinetic study. Table 1 depicts the linear forms of three kinetic models including all kinetic parameters for comparing pseudo-first-order, pseudo-second-order, and intra-particle diffusion models in terms of correlation coefficients. It is very evident that pseudo-second-order model has higher correlation coefficient than pseudo-first-order model and also the calculated adsorption capacity $Q_e$ of pseudo-second-order model was much more closer to the experimental adsorption

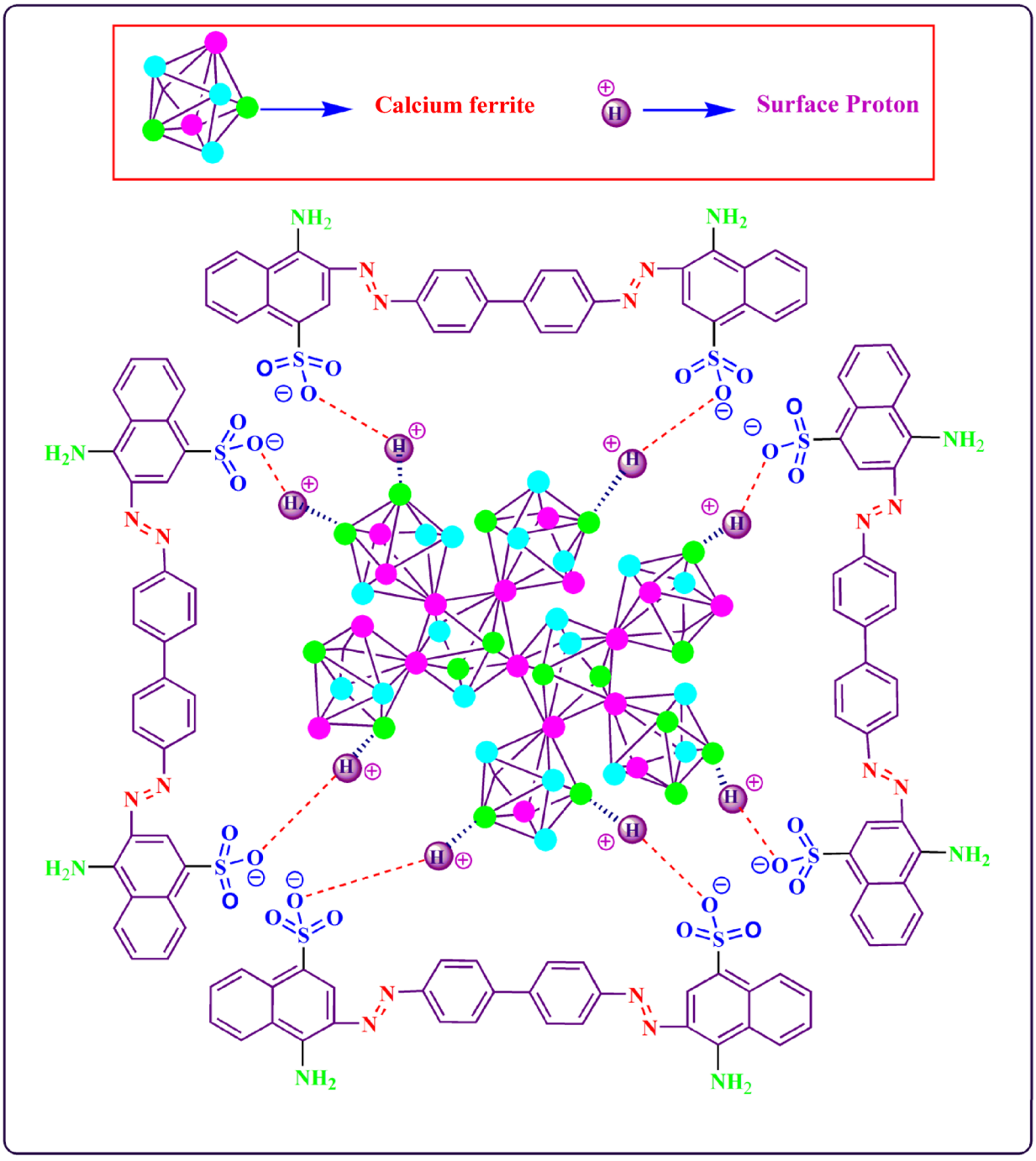


Fig. 5. Schematic diagram showing the electrostatic attraction between anionic CR dye molecules toward protonated $CaFe_2O_4$ nanoparticles.

capacity $Q_e$(exp) for various CR concentrations, confirming better applicability of pseudo-second-order model compared with pseudo-first-order model. The very good fitting of adsorption experimental data with linear form of pseudo-second-order kinetic model is depicted in Fig. 8(a). Thus, it indicates that the adsorption of CR dye onto $CaFe_2O_4$ nanoparticles is a chemisorption process [33,34].

Weber–Morris model was also studied to analyze the contribution of intra-particle diffusion in this adsorption process. The plot of $q_t$ (mg/g) vs. $t^{0.5}$ for three different initial CR concentrations (20, 40, and 60 mg/L) is shown in Fig. 8(b). Weber–Morris model is always characterized with multi-linearity which explains the three stages of adsorption through intra-particle diffusion where diffusion adsorption is the first stage followed by intra-particle diffusion at the pores available and ended by the equilibrium stage where no more adsorbate can be accommodated [35]. The plot (Fig. 8(b)) clearly indicates that experimental data

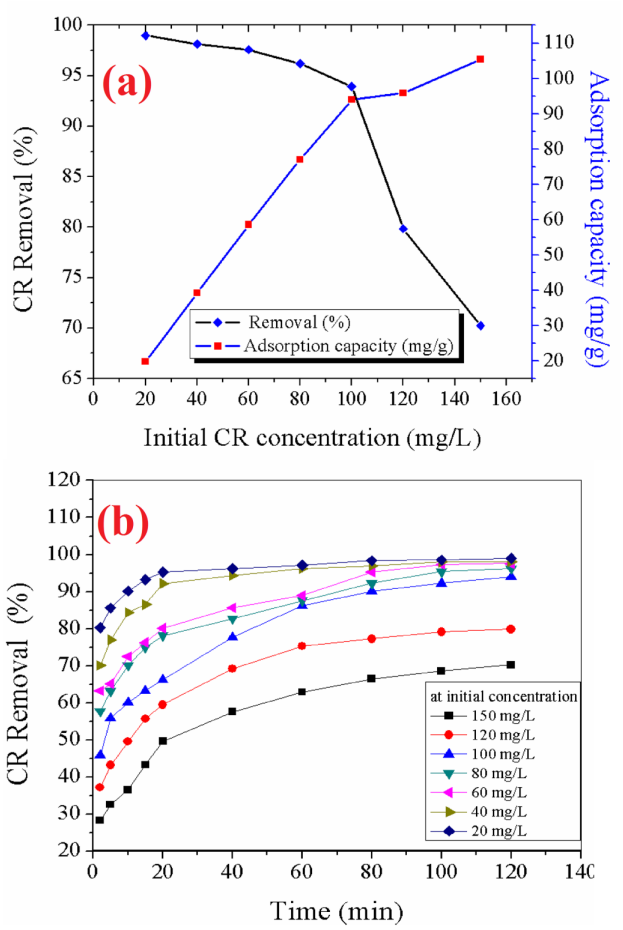


Fig. 6. Plot showing the (a) effect of initial concentration of CR dye onto its removal efficiency and (b) effect of contact time on the CR adsorption efficiency.

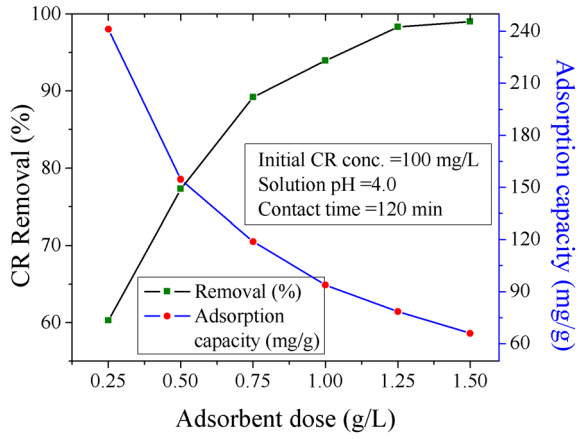


Fig. 7. Plot showing the effect of adsorbent dose on the adsorption of CR dye.

can be fitted with two linear portions but none of them passes through the origin, that is, intra-particle diffusion is not the sole rate-limiting step [30]. Hence, external mass transfer might also play an important role in controlling the adsorption rate. All the correlation coefficient values from Weber–Morris model (Table 1) are in the range of 0.910–0.984, which is lower than that of second-order kinetic model (0.999–1.000). Hence, adsorption kinetic of CR dye onto $CaFe_2O_4$ nanoparticle was found to strictly follow pseudo-second-order model and the intra-particle diffusion was not the sole rate-limiting step, while the external mass transfer might also play an important role in controlling the adsorption rate in this adsorption process [30,36].

### 3.6. Isotherm modeling

Isotherm studies also play a major role in designing the application part of any adsorbent in terms of adsorption capacity and favorability of the adsorption process. It gives the detail about the adsorption capacity (mg of adsorbate/g of adsorbent) of an adsorbent at equilibrium. In isotherm modeling studies, various initial CR dye concentration (20–60 mg/L) with different $CaFe_2O_4$ nanoparticles doses (0.25–1.0 g/L) at optimized solution pH 4.0 and at room temperature were considered. Linear forms of conventional isotherm models like Langmuir and Freundlich were used to fit the equilibrium data and the corresponding isotherm parameters with their linear form are presented in Table 2. The comparison between the models with respect to the correlation coefficient yielded that the Langmuir model have better fitting ($R^2$: 0.981–0.993) compared with Freundlich isotherm model ($R^2$: 0.881–0.969). The favorability factor of Langmuir isotherm ($R_L$) was also calculated, which was in the range of 0.013–0.076, indicates the highly favorable nature of CR adsorption onto $CaFe_2O_4$ nanoparticles. In case of Freundlich isotherm, the parameter, $K_F$ ($mg^{(1-1/n)}\ L^{1/n}\ g^{-1}$) represents the adsorption capacity of adsorbent and the parameter "1/*n*" is a dimensionless factor which indicates the adsorption intensity. In this case, 1/*n* values for all considered doses of adsorbent were found to be less than unity, which also implies the favorability of this adsorption process. Hence, CR dye was adsorbed onto $CaFe_2O_4$ nanoparticles as a monolayer in a homogenous favorable system rather on a heterogeneous energy system and having maximum adsorption capacity of 241.16 mg/g for CR dye.

### 3.7. Comparison with other adsorbents

A performance comparison in terms of adsorption capacities of similar type of adsorbents used for CR dye removal is drawn with our prepared adsorbent and is presented in Table 3. It can be seen that the adsorbent reported in this study in comparison with all of the other adsorbents are preferable or comparable in terms of its adsorption capacity. Hence, $CaFe_2O_4$ nanoparticles with high adsorption capacity toward CR dye along with easy magnetic separation ability, high surface area, and availability of more active adsorption sites makes it as preferable and superior one for dye removal from aqueous solution.

### 3.8. Prediction modeling by ANN

ANN is a very popular modeling tool inspired by human brain and nervous systems that are known for their high capability to learn and classify data. The neural networks

Table 1
Kinetic parameters for CR dye removal onto $CaFe_2O_4$ nanoparticles (dose: 1.0 g/L) over initial CR dye concentrations of 20-60 mg/L

| Models | Linear form | Parameters | CR dye concentration (mg/L) | | |
|---|---|---|---|---|---|
| | | | 20 | 40 | 60 |
| First-order kinetic | $\log(Q_e - Q_t) = \log Q_e - \frac{k_f}{2.303}t$ | $k_f$ | 0.035 | 0.044 | 0.039 |
| | | $Q_e$ | 2.535 | 9.462 | 26.303 |
| | | $R^2$ | 0.946 | 0.959 | 0.959 |
| Second-order kinetic | $\frac{t}{Q_t} = \frac{1}{k_s Q_e^2} + \frac{1}{Q_e}t$ | $k_s$ | 0.047 | 0.015 | 0.004 |
| | | $Q_e$ | 21.27 | 40.01 | 61.50 |
| | | $R^2$ | 1.000 | 0.999 | 0.999 |
| | | $h$ | 21.26 | 24.01 | 15.13 |
| Intra-particle diffusion | $Q_t = k_{id}t^{1/2} + c$ | $k_{id1}$ | 0.979 | 2.774 | 3.475 |
| | | $R_1^2$ | 0.984 | 0.980 | 0.972 |
| | | $c_2$ | 18.494 | 35.808 | 40.812 |
| | | $k_{id2}$ | 0.122 | 0.328 | 1.699 |
| | | $R_2^2$ | 0.942 | 0.940 | 0.910 |
| Experimental value | | $Q_e$ (exp) | 19.796 | 39.26 | 58.554 |

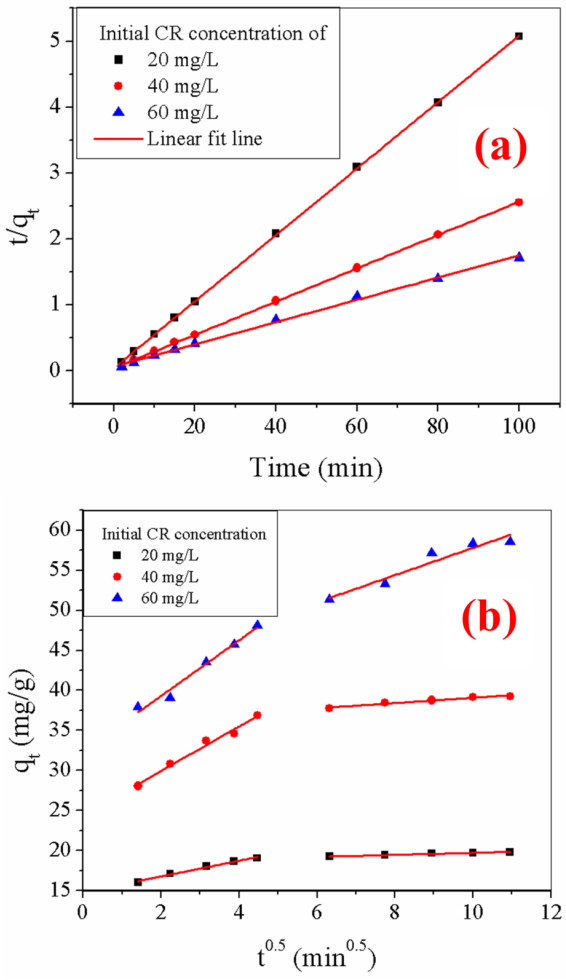


Fig. 8. (a) Linear fitting of pseudo-second-order kinetic model, (b) multi-linear fitting of intra-particle diffusion model for CR dye adsorption onto $CaFe_2O_4$ nanoparticles.

are constituted of different simple elements like input layer, hidden layer, and output layer with numbers of neurons in each layer which are operating in parallel. An ANN can be trained by altering the weight values in between neurons of two subsequent layers [45] and the main objective of training is to obtain the desired output for known inputs [46,47]. Hence, the training of network continued until the network output shows good agreement with the target. Although ANNs have wide applicability in all field of research since last two decades or so, recently this technique is also widely used for predicting the efficiency of various chemical modeling processes including predicting adsorption efficiency of an adsorbent in solid–liquid interaction in adsorption system [48]. In the present study, a three layer feed forward back-propagation ANN model was developed with solution pH, $CaFe_2O_4$ nanoparticles dose, contact time, and initial CR dye concentration as input variables and the CR dye removal efficiency obtained from batch experiments were considered as target of the model. The typical ANN architecture used in this study is shown in Fig. 9(a). The experimental data obtained at different values of experimental parameters such as solution pH (4.0–10.0), contact time (2–120 min), adsorbent dose (0.25–1.5 g/L), and initial CR dye concentration (20–150 mg/L) were used for ANN modeling. Prediction of the removal efficiency of CR dye was performed using Neural Network Toolbox of MATLAB (R2014a) mathematical software. A total of 159 data points were used for ANN model training and the data points were randomly separated into three categories (70% for training, 15% for testing, and 15% for validation). Hence, 111, 24, and 24 data points were used for training, testing, and validation of the ANN models, respectively. All the experimental data for inputs and output were normalized in the range of 0–1 using Eq. (1) to avoid numerical overflows on account of introduction of exceptionally high or low weights:

$$Y_i = \frac{\left(X_i - X_{\min}\right)}{X_{\max} - X_{\min}} \quad (1)$$

Table 2
Adsorption isotherm constants for adsorption of CR dye onto $CaFe_2O_4$ nanoparticles

| Isotherm | Linear form | Parameters | $CaFe_2O_4$ nanoparticle dose (g/L) | | | |
|---|---|---|---|---|---|---|
| | | | 0.25 | 0.5 | 0.75 | 1.0 |
| Langmuir | $\frac{C_e}{Q_e}=\frac{1}{Q_m b}+\frac{C_e}{Q_m}$ | $Q_m$ (mg/g) | 241.16 | 173.25 | 123.26 | 90.91 |
| | | $b$ (L/mg) | 0.653 | 0.758 | 0.923 | 1.236 |
| | | $R_L$ | 0.076-0.025 | 0.066-0.022 | 0.054-0.018 | 0.040-0.013 |
| | | $R^2$ | 0.993 | 0.989 | 0.981 | 0.985 |
| Freundlich | $\ln Q_e=\ln K_F+\frac{1}{n}\ln C_e$ | $1/n$ | 0.4504 | 0.4608 | 0.4975 | 0.5494 |
| | | $K_F$ ($mg^{(1-1/n)}\,L^{1/n}\,g^{-1}$) | 17.027 | 9.125 | 6.352 | 3.039 |
| | | $R^2$ | 0.883 | 0.915 | 0.8815 | 0.969 |

Table 3
Comparison between the present study and other adsorbents in terms of adsorption capacity for CR dye adsorption

| Adsorbent | Adsorption capacity (mg/g) | Reference |
|---|---|---|
| $CoFe_2O_4$ nanoparticles | 93.74 | [20] |
| $Ni_{0.5}Zn_{0.5}Fe_2O_4$ nanopowders | 204.82 | [21] |
| $Ni_{0.6}Fe_{2.4}O_4$ nanoparticles | 72.73 | [35] |
| Gadolinium-doped cobalt ferrite nanoparticles | 263.16 | [37] |
| Nanocrystalline $Fe_2O_3$ | 203.66 | [38] |
| $MnFe_2O_4$ nanoparticles | 92.40 | [39] |
| Zinc oxide nanorods loaded on activated carbon | 142.90 | [40] |
| Palladium nanoparticles loaded on activated carbon | 76.9 | [40] |
| Chitosan | 320.00 | [41] |
| Maghemite nanoparticles | 208.33 | [42] |
| Bentonite | 158.70 | [43] |
| Bimetallic Fe–Zn nanoparticles | 28.56 | [44] |
| $CaFe_2O_4$ nanoparticles | 241.16 | In this study |

where $Y_i$ is the normalized value of $X_i$, $X_{max}$, and $X_{min}$ are the maximum and minimum values of $X_i$, respectively [49]. While developing the neural networks, popular tangent sigmoid transfer function (tansig) was used in between input and hidden layer and linear transfer function (purelin) was used in between hidden and output layer. It is very important to select a suitable algorithm and training function in order to get the desired output. In this work, backpropagation algorithm "Levenberg–Marquardt" with 1,000 iterations was used for training the neural network considering the wide applicability of this algorithm in chemical modeling. Optimization of the ANN architecture was performed by changing the number of neurons in the hidden layer in a range of 1–20 and subsequently 20 different networks were developed. In order to study the potentiality of the 20 different models for predicting the CR dye removal efficiency, two important criteria such as mean squared error (MSE) and coefficient of determination ($R^2$) were used [49] as mentioned in Eqs. (2) and (3), respectively:

$$\mathrm{MSE}=\frac{1}{N}\sum_{i=1}^{N}\left(\left|Y_{\mathrm{Prd},i}-Y_{\mathrm{Exp},i}\right|\right)^2 \tag{2}$$

$$R^2=1-\frac{\sum_{i=1}^{N}\left(Y_{\mathrm{Prd},i}-Y_{\mathrm{Exp},i}\right)}{\sum_{i=1}^{N}\left(Y_{\mathrm{Prd},i}-Y_{\mathrm{mean}}\right)} \tag{3}$$

where $Y_{\mathrm{Prd},i}$ represents the model predicted value, $Y_{\mathrm{Exp},i}$ represents the experimental value used for modeling, $N$ indicates the number of data points, and $Y_{\mathrm{mean}}$ represents the arithmetic mean value of all experimental data points.

The batch mode adsorption experimental data obtained under different operating conditions was used to train and test the neural network model for CR dye prediction modeling in this work. A total of 20 different models were developed by changing the number of neurons in the hidden layer and the best model was chosen based on the minimum value of MSE and maximum value of $R^2$ value of training, testing, and validation data set. The variation of $R^2$ and MSE values for training, testing, and validation data set due to change in neuron number in the hidden layer is depicted in Table 4. Moreover, the variation of MSE with number of neurons at hidden layer is shown in Fig. 9(b), which clearly shows that for the network with nine neurons in the hidden layer the MSE reaches its lowest value and thereafter increasing trend in MSE value was observed with 10 or more number of neurons. The network with nine neurons at the hidden layer with an MSE value of 0.00042866 for validation data set was chosen to be the best one. The potentiality of the optimal network with nine neurons at hidden layer is conformed for accurately predicting the CR dye removal efficiency on account of its very small MSE value and very high $R^2$ value for validation data set. The test outputs showed little deviation from the experimental data in terms of normalized uptake efficiency with an average value of 0.00042866. The variation of MSE with number of epochs for optimal network is shown in Fig. 9(c), which shows that training was stopped only after 41 epochs as the best validation performance was obtained at that epoch, indicating high converging efficiency of the model. Hence, ANN model with four inputs (pH, adsorbent dosage, contact time, and initial concentration of CR solution), nine neurons at hidden layer and

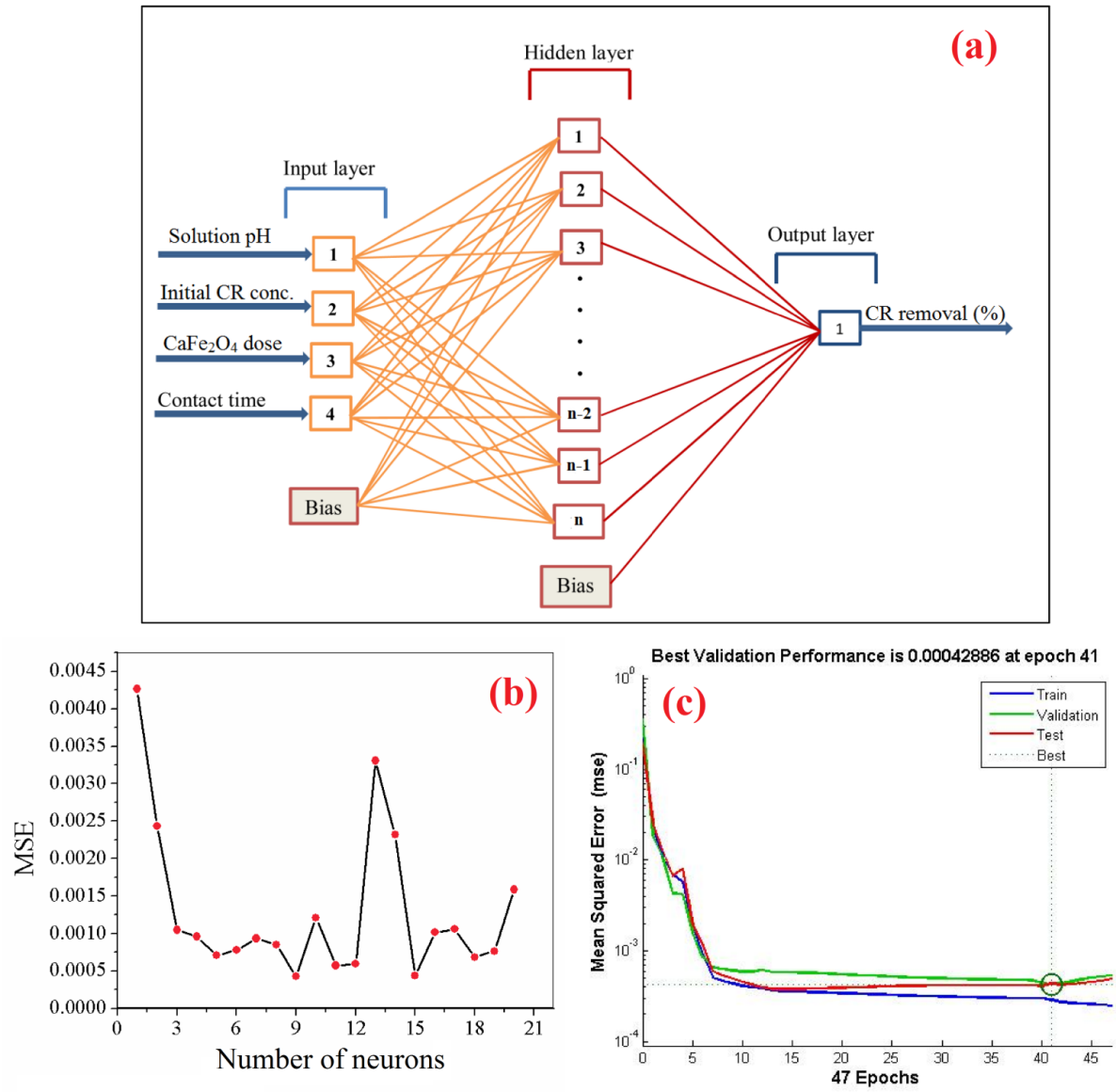


Fig. 9. Plot showing the (a) three layer optimal ANN architecture obtained for this study, (b) dependence between MSE with number of neurons at hidden layer for determining optimal ANN architecture, and (c) variation of MSE with epochs during optimization of ANN architecture.

CR dye removal efficiency as the output becomes the optimum one with architecture of 4-9-1. Thereafter the optimal model was utilized for prediction modeling and a regression analysis of the model predicted normalized values with normalized experimental values were performed. The graphical representation of regression analysis between normalized ANN outputs vs. normalized experimental data is shown in Fig. 10(a), which exhibits very close agreement between them. The weights and bias values for the optimal network were also obtained and are depicted in Table 5, which were used further for sensitivity analysis.

### 3.9. Sensitivity analysis

In order to evaluate the influence of four input parameters onto CR removal efficiency a sensitivity analysis was performed using the neural weight data (Table 5) employing the technique of connection weight partitioning methodology using Eq. (4) [50]:

$$R = \frac{\sum_{j=1}^{h}\left[\left(\frac{|IW_{ij}|}{\sum_{k=1}^{m}|IW_{kj}|}\right)|LW_j|\right]}{\sum_{j=1}^{m}\left\{\sum_{j=1}^{h}\left[\left(\frac{|IW_{ij}|}{\sum_{k=1}^{m}|IW_{kj}|}\right)LW_j\right]\right\}} \tag{4}$$

where $R$ represents the relative importance of four input variables, $m$ and $h$ indicates the number of neurons in input and hidden layer of the optimal network, respectively.

The result of sensitivity analysis is shown in Fig. 10(b), which clearly depicts that the solution pH is most critical input parameter (41%) after that $CaFe_2O_4$ dose (29%) and initial CR dye concentration (24%). However, the input parameter contact time has minimum impact on the CR removal efficiency. The results of the sensitivity analysis are in agreement with the experimental results (Figs. 4(a) and 6(b)), which depicts high dependency of this adsorption process onto solution pH and relatively insignificant effect of contact time on CR dye removal efficiency after 20 min of contact time or so.

Table 4
The variation of MSE and $R^2$ values during optimization of ANN architecture

| Network number | Training ($R^2$) | Testing ($R^2$) | Validation | | All data |
|---|---|---|---|---|---|
| | | | $R^2$ | MSE | |
| 1 | 0.944 | 0.947 | 0.946 | 0.0042656 | 0.944 |
| 2 | 0.970 | 0.988 | 0.972 | 0.0024352 | 0.972 |
| 3 | 0.987 | 0.975 | 0.989 | 0.0010486 | 0.985 |
| 4 | 0.988 | 0.956 | 0.993 | 0.00096033 | 0.984 |
| 5 | 0.990 | 0.990 | 0.992 | 0.00070889 | 0.991 |
| 6 | 0.980 | 0.978 | 0.990 | 0.00078254 | 0.981 |
| 7 | 0.994 | 0.985 | 0.987 | 0.00093406 | 0.992 |
| 8 | 0.985 | 0.970 | 0.990 | 0.0008523 | 0.982 |
| 9 | 0.995 | 0.994 | 0.992 | 0.00042886 | 0.995 |
| 10 | 0.993 | 0.991 | 0.982 | 0.0012128 | 0.991 |
| 11 | 0.992 | 0.989 | 0.991 | 0.000573 | 0.991 |
| 12 | 0.991 | 0.984 | 0.990 | 0.00059656 | 0.990 |
| 13 | 0.984 | 0.969 | 0.991 | 0.0033085 | 0.988 |
| 14 | 0.990 | 0.985 | 0.967 | 0.002321 | 0.986 |
| 15 | 0.991 | 0.989 | 0.994 | 0.0004362 | 0.996 |
| 16 | 0.988 | 0.981 | 0.990 | 0.0010185 | 0.987 |
| 17 | 0.992 | 0.985 | 0.987 | 0.0010609 | 0.990 |
| 18 | 0.990 | 0.990 | 0.991 | 0.00068623 | 0.990 |
| 19 | 0.991 | 0.991 | 0.991 | 0.00076564 | 0.991 |
| 20 | 0.991 | 0.963 | 0.979 | 0.0015858 | 0.983 |

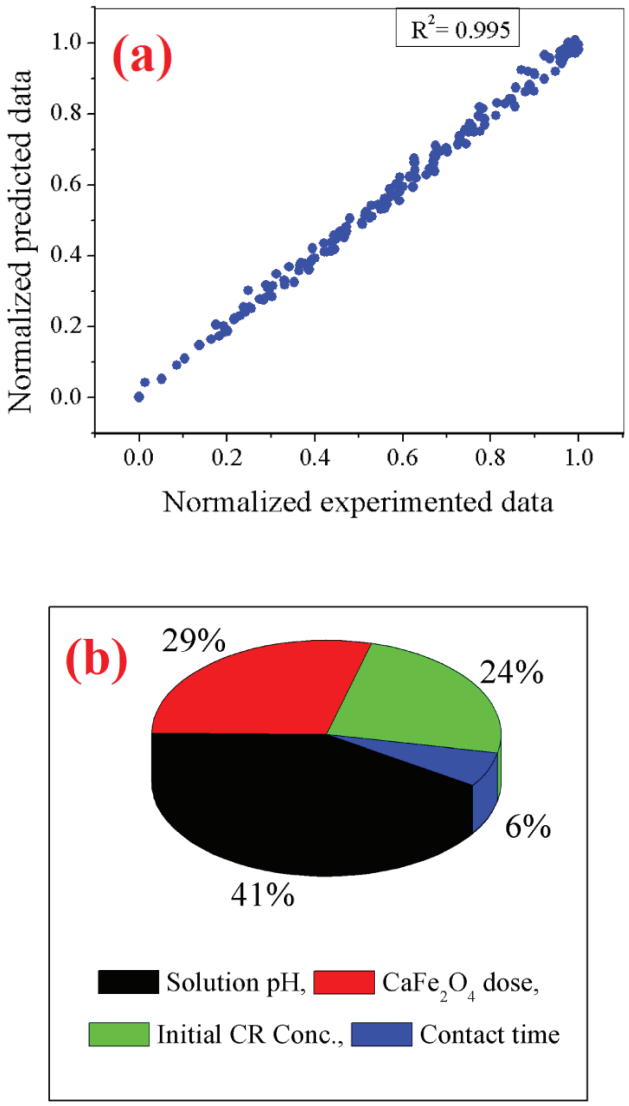


Fig. 10. (a) The linear regression between ANN model predicted data vs. experimental data and (b) the influence of input experimental parameters on CR removal as obtained by sensitivity analysis.

Table 5
The weight and bias values of hidden and output layer for optimal ANN architecture

| Hidden layer weights | | | | Output layer weights | Hidden layer bias | Output layer bias |
|---|---|---|---|---|---|---|
| 2.01 | 1.4088 | 0.27041 | –1.7216 | 1.5659 | –0.59903 | –1.1936 |
| –1.9502 | 0.47662 | 0.27008 | –1.472 | 0.48536 | –0.76197 | |
| 0.86534 | 1.1968 | 0.45572 | –1.6287 | –1.9015 | –0.010699 | |
| 2.6751 | 0.95007 | 0.25694 | –1.0699 | –1.2954 | 0.57444 | |
| –0.72812 | –0.44115 | –3.3272 | 0.094577 | –0.16198 | –0.52389 | |
| 1.6704 | 1.4169 | –0.099241 | –2.072 | 1.4312 | 0.60728 | |
| –0.32785 | 0.16538 | 0.69956 | 2.522 | 0.33852 | –1.4178 | |
| –0.18063 | –0.051981 | –3.1184 | –0.005008 | –2.0042 | –4.0877 | |
| 0.74577 | 0.87744 | 2.6996 | –1.2388 | 0.17933 | 2.0752 | |

## 4. Conclusion

The $CaFe_2O_4$ nanoparticles synthesized by simple precipitation method showed a high adsorptive efficiency toward toxic CR dye with maximum adsorption capacity of 241.16 mg/g at optimum condition. The adsorption process performance was highly pH dependent and maximum CR dye uptake efficiency of ~99% was reported at solution pH 4.0. The adsorption process of CR dye onto $CaFe_2O_4$ nanoparticles was governed by pseudo-second-order kinetic model, and intra-particle diffusion is not the only rate-limiting step. CR was adsorbed as a monolayer in a homogeneous system which is justified by isotherm studies having a better fit with Langmuir isotherm model. Optimum ANN model with nine neurons in the hidden layer (4-9-1) and Levenberg–Marquardt backpropagation algorithm with "tansig" in the hidden layer and "purelin" in the output layer was most suitable to predict the CR dye uptake efficiency. Results obtained from the neural model, showed that the values of the determination coefficient ($R^2$) and the MSE were found to be 0.995 and 0.00042866, respectively, for CR dye adsorption. Thus, it can be concluded that the $CaFe_2O_4$ nanoparticles are a viable and potential adsorbent for removal of CR dye from dye contaminated wastewater and could be tried with other threat possessing water pollutants.

## Acknowledgment

The authors are thankful to Central Research Facility (CRF) of National Institute of Technology Agartala for extending XRD and UV-Vis-NIR spectroscopic measurement facilities.

## References

[1] H.J. Kumari, P. Krishnamoorthy, T.K. Arumugam, S. Radhakrishnan, D. Vasudevan, An efficient removal of crystal violet dye from wastewater by adsorption onto TLAC/chitosan composite: a novel low cost adsorbent, Int. J. Biol. Macromol., 96 (2017) 324–333.

[2] F. Rehman, P.L.O. Volpe, C. Airoldi, Free amino and imino-bridged centres attached to organic chains bonded to structurally ordered silica for dye removal from aqueous solution, J. Environ. Manage., 133 (2014) 135–143.

[3] Y.Z. Zhang, J. Li, J. Zhao, W. Bian, Y. Li, X.J. Wang, Adsorption behavior of modified Iron stick yam skin with polyethyleneimine as a potential biosorbent for the removal of anionic dyes in single and ternary systems at low temperature, Bioresour. Technol., 222 (2016) 285–293.

[4] P. Vairavel, R.V. Murty, S. Nethaji, Removal of Congo red dye from aqueous solutions by adsorption onto a dual adsorbent (*Neurosporacrassa* dead biomass and wheat bran): optimization, isotherm, and kinetics studies, Desal. Wat. Treat., 68 (2017) 274–292.

[5] A. Mittal, V. Thakur, J. Mittal, H. Vardhan, Process development for the removal of hazardous anionic azo dye Congo red from wastewater by using hen feather as potential adsorbent, Desal. Wat. Treat., 52 (2014) 227–237.

[6] N.P. Raval, P.U. Shah, N.K. Shah, Adsorptive amputation of hazardous azo dye Congo red from wastewater: a critical review, Environ. Sci. Pollut. Res., 23 (2016) 14810–14853.

[7] M.K. Nayunigari, R. Das, A. Maity, S. Agarwal, V.K. Gupta, Folic acid modified cross-linked cationic polymer: synthesis, characterization and application of the removal of Congo red dye from aqueous medium, J. Mol. Liq., 227 (2017) 87–97.

[8] M.H. Beyki, H. Alijani, Y. Fazli, Solvent free synthesized $MnFe_2O_4$@polyamid resin as a novel green nanohybrid for fast removing Congo red, J. Mol. Liq., 216 (2016) 6-11.

[9] W.T. Mook, M.K. Aroua, M. Szlachta, C.S. Lee, Optimisation of Reactive Black 5 dye removal by electrocoagulation process using response surface methodology, Water Sci. Technol., 75 (2017) 952–962.

[10] P. Zhang, X. Yang, Z. Zhao, B. Li, J. Gui, D. Liu, J. Qiu, One-step synthesis of flowerlike C/$Fe_2O_3$ nanosheet assembly with superior adsorption capacity and visible light photocatalytic performance for dye removal, Carbon, 116 (2017) 59–67.

[11] K. Vijayaraghavan, Y. Premkumar, J. Jegan, Malachite green and crystal violet biosorption onto coco-peat: characterization and removal studies, Desal. Wat. Treat., 57 (2016) 6423–6431.

[12] L. Yang, Z. Wang, J. Zhang, Zeolite imidazolate framework hybrid nanofiltration (NF) membranes with enhanced perm selectivity for dye removal, J. Membr. Sci., 532 (2017) 76–86.

[13] A. Debnath, K. Deb, K.K. Chattopadhyay, B. Saha, Methyl orange adsorption onto simple chemical route synthesized crystalline $\alpha$-$Fe_2O_3$ nanoparticles: kinetic, equilibrium isotherm, and neural network modeling, Desal. Wat. Treat., 57 (2016) 13549-13560.

[14] Y.J. Zhang, J.L. Ou, Z.K. Duan, Z.J. Xing, Y. Wang, Adsorption of Cr(VI) on bamboo bark-based activated carbon in the absence and presence of humic acid, Colloids Surf., A, 481 (2015) 108-116.

[15] R. Chug, V.S. Gour, S. Mathur, S.L. Kothari, Optimization of extracellular polymeric substances production using *Azotobacter beijreinckii* and *Bacillus subtilis* and its application in chromium (VI) removal, Bioresour. Technol., 214 (2016) 604–608.

[16] A.R. Esfahani, S. Hojati, A. Azimi, M. Farzadian, A. Khataee, Enhanced hexavalent chromium removal from aqueous solution using a sepiolite-stabilized zero-valent iron nanocomposite: impact of operational parameters and artificial neural network modeling, J. Taiwan Inst. Chem. Eng., 49 (2015) 172–182.

[17] G. Sharma, M. Naushad, D. Pathania, A. Mittal, G.E. El-desoky, Modification of *Hibiscus cannabinus* fiber by graft copolymerization: application for dye removal, Desal. Wat. Treat., 54 (2015) 3114–3121.

[18] S. Gita, S.P. Shukla, T.G. Choudhury, C. Prakash, A.R. Singh, A prototype of novel agro-waste based column bed device for removal of textile dye Optilan Red, Water Sci. Technol., (2017). 76 (2017) 1251–1260.

[19] D.D. Sewu, P. Boakye, S.H. Woo, Highly efficient adsorption of cationic dye by biochar produced with Korean cabbage waste, Bioresour. Technol., 224 (2017) 206–213.

[20] R. Liu, Y. Tian, J. Xu, H. Fu, Y. Li, Efficient removal of Congo Red by magnetic $CoFe_2O_4$ nanoparticles prepared via the rapid combustion process, J. Nanosci. Nanotechnol., 16 (2016) 9535–9543.

[21] R. Liu, H. Fu, H. Yin, P. Wang, L. Lu, Y. Tao, A facile sol combustion and calcinations process for the preparation of magnetic $Ni_{0.5}Zn_{0.5}Fe_2O_4$ nanopowders and their adsorption behaviors of Congo red, Powder Technol., 274 (2015) 418–425.

[22] R. Liu, P. Lv, H. Fu, R. Lu, X. Wu, Y. Lu, Removal performance of Methyl Blue onto magnetic $MgFe_2O_4$ nanoparticles prepared via the rapid combustion process, J. Nanosci. Nanotechnol., 17 (2017) 4755–4762.

[23] A. Debnath, M. Majumder, M. Pal, N.S. Das, K.K. Chattopadhyay, B. Saha, Enhanced adsorption of hexavalent chromium onto magnetic calcium ferrite nanoparticles: kinetic, isotherm, and neural network modeling, J. Dispersion Sci. Technol., 37 (2016) 1806–1818.

[24] D. Ghanbari, M. Salavati-Niasari, F. Beshkar, O. Amiri, Electro-spinning of cellulose acetate nanofibers: microwave synthesize of calcium ferrite nanoparticles and CA–Ag–$CaFe_2O_4$ nanocomposites, J. Mater. Sci. - Mater. Electron., 26 (2015) 8358–8366.

[25] L. Shao, Z. Ren, G. Zhang, L. Chen, Facile synthesis, characterization of a $MnFe_2O_4$/activated carbon magnetic composite and its effectiveness in tetracycline removal, Mater. Chem. Phys., 135 (2012) 16–24.

[26] S. Dhanavel, E.A.K. Nivethaa, K. Dhanapal, V.K. Gupta, V. Narayanan, A. Stephen, $\alpha$-$MoO_3$/polyaniline composite for effective scavenging of Rhodamine B, Congo red and textile dye effluent, RSC Adv., 6 (2016) 28871–28886.
[27] O. Ozdemir, B. Armagan, M. Turan, M.S. Celik, Comparison of the adsorption characteristics of azo-reactive dyes on mezoporous minerals, Dyes Pigm., 62 (2004) 49–60.
[28] X. Liu, Z. Zhang, W. Shi, Y. Zhang, S. An, L. Zhang, Adsorbing properties of magnetic nanoparticles Mn-ferrites on removal of Congo Red from aqueous solution, J. Dispersion Sci. Technol., 36 (2015) 462-470.
[29] R. Kumar, M.O. Ansari, N. Parveen, M.A. Barakat, M.H. Cho, Simple route for the generation of differently functionalized PVC@ graphene–polyaniline fiber bundles for the removal of Congo red from wastewater, RSC Adv., 5 (2015) 61486–61494.
[30] J. Shu, Z. Wang, Y. Huang, N. Huang, C. Ren, W. Zhang, Adsorption removal of Congo red from aqueous solution by polyhedral $Cu_2O$ nanoparticles: kinetics, isotherms, thermodynamics and mechanism analysis, J. Alloys Compd., 633 (2015) 338–346.
[31] M. Ghaedi, M.R. Rahimi, A.M. Ghaedi, I. Tyagi, S. Agarwal, V.K. Gupta, Application of least squares support vector regression and linear multiple regression for modeling removal of methyl orange onto tin oxide nanoparticles loaded on activated carbon and activated carbon prepared from *Pistaciaatlantica* wood, J. Colloid Interface Sci., 461 (2016) 425–434.
[32] S. Shahabuddin, N.M. Sarih, S. Mohamad, S.N.A. Baharin, Synthesis and characterization of $CO_3O_4$ nanocube-doped polyaniline nanocomposites with enhanced methyl orange adsorption from aqueous solution, RSC Adv., 6 (2016) 43388–43400.
[33] J. Dai, J. Sun, A. Xie, J. He, C. Li, Y. Yan, Designed preparation of 3D hierarchically porous carbon material via solvothermal route and in situ activation for ultrahigh-efficiency dye removal: adsorption isotherm, kinetics and thermodynamics characteristics, RSC Adv., 6 (2016) 3446–3457.
[34] E. Rosales, M. Pazos, M.A. Sanroman, T. Tavares, Application of zeolite-*Arthrobacter viscous* system for the removal of heavy metal and dye: chromium and Azure B, Desalination, 284 (2012) 150–156.
[35] S. Zeng, S. Duan, R. Tang, L. Li, C. Liu, D. Sun, Magnetically separable $Ni_{0.6}Fe_{2.4}O_4$ nanoparticles as an effective adsorbent for dye removal: synthesis and study on the kinetic and thermodynamic behaviors for dye adsorption, Chem. Eng. J., 258 (2014) 218-228.
[36] S. An, X. Liu, L. Yang, L. Zhang, Enhancement removal of crystal violet dye using magnetic calcium ferrite nanoparticle: study in single- and binary-solute systems, Chem. Eng. Res. Des., 94 (2015) 726-735.
[37] X. Zhao, W. Wang, Y. Zhang, S. Wu, F. Li, J.P. Liu, Synthesis and characterization of gadolinium doped cobalt ferrite nanoparticles with enhanced adsorption capability for Congo Red, Chem. Eng. J., 250 (2014) 164-174.
[38] A. Debnath, K. Deb, N.S. Das, K.K. Chattopadhyay, B. Saha, Simple chemical route synthesis of $Fe_2O_3$ nanoparticles and its application for adsorptive removal of Congo Red from aqueous media: artificial neural network modeling, J. Dispersion Sci. Technol., 37 (2016) 775-785.
[39] L. Wang, J. Li, Y. Wang, L. Zhao, Q. Jiang, Adsorption capability for Congo red on nanocrystalline $MFe_2O_4$ (M = Mn, Fe, Co, Ni) spinel ferrites, Chem. Eng. J., 181 (2012) 72–79.
[40] M. Ghaedi, M.N. Biyareh, S.N. Kokhdan, S. Shamsaldini, R. Sahraei, A. Daneshfar, S. Shahriyar, Comparison of the efficiency of palladium and silver nanoparticles loaded on activated carbon and zinc oxide nanorods loaded on activated carbon as new adsorbents for removal of Congo red from aqueous solution: kinetic and isotherm study, Mater. Sci. Eng., C, 32 (2012) 725–734.
[41] A. Zúñiga-Zamora, J. García-Mena, E. Cervantes-González, Removal of Congo Red from the aqueous phase by chitin and chitosan from waste shrimp, Desal. Wat. Treat., 57 (2016) 14674–14685.
[42] A. Afkhami, R. Moosavi, Adsorptive removal of Congo red a carcinogenic textile dye from aqueous solutions by maghemite nanoparticles, J. Hazard. Mater., 174 (2010) 398–403.
[43] E. Bulut, M. Özacar, I.A. Sengil, Equilibrium and kinetic data and process design for adsorption of Congo Red onto bentonite, J. Hazard. Mater., 154 (2008) 613–622.
[44] R.K. Gautam, V. Rawat, S. Banerjee, M.A. Sanroman, S. Soni, S.K. Singh, M.C. Chattopadhyaya, Synthesis of bimetallic Fe–Zn nanoparticles and its application towards adsorptive removal of carcinogenic dye malachite green and Congo red in water, J. Mol. Liq., 212 (2015) 227–236.
[45] F.N. Azad, M. Ghaedi, A. Asfaram, A. Jamshidi, G. Hassani, A. Goudarzi, A. Ghaedi, Optimization of the process parameters for the adsorption of ternary dyes by Ni doped FeO(OH)-NWs–AC using response surface methodology and an artificial neural network, RSC Adv., 6 (2016) 19768–19779.
[46] A. Debnath, M. Majumder, M. Pal, A cognitive approach in selection of source for water treatment plant based on climatic impact, Water Resour. Manage., 29 (2015) 1907–1919.
[47] A. Celekli, S.S. Birecikligil, F. Geyik, H. Bozkurt, Prediction of removal efficiency of Lanaset Red G on walnut husk using artificial neural network model, Bioresour. Technol., 103 (2012) 64–70.
[48] H.A. Hamid, Y. Jenidi, W. Thielemans, C. Somerfield, R.L. Gomes, Predicting the capability of carboxylated cellulose nanowhiskers for the remediation of copper from water using response surface methodology (RSM) and artificial neural network (ANN) models, Ind. Crops Prod., 93 (2016) 108–120.
[49] K.L. Bhowmik, A. Debnath, R.K. Nath, S. Das, K.K. Chattopadhyay, B. Saha, Synthesis and characterization of mixed phase manganese ferrite and hausmannite magnetic nanoparticle as potential adsorbent for methyl orange from aqueous media: artificial neural network modeling, J. Mol. Liq., 219 (2016) 1010–1022.
[50] M. Khajeh, A.R. Golzary, Synthesis of zinc oxide nanoparticles–chitosan for extraction of methyl orange from water samples: cuckoo optimization algorithm–artificial neural network, Spectrochim. Acta, Part A, 131 (2014) 189–194.